Superlattice formed by quantum-dot sheets: Density of states and infrared absorption

F. T. Vasko* and V. V. Mitin
Department of Electrical Engineering, University at Buffalo, Buffalo, New York 14260-1920, USA
(Received 23 March 2012; published 28 June 2012)

Low-energy continuous states of electron in a heterosrtucture with periodically placed quantum-dot sheets are studied theoretically. The Green's function of an electron is governed by the Dyson equation with the self-energy function which is determined the boundary conditions at quantum-dot sheets with weak damping in the low-energy region. The parameters of a superlattice formed by quantum-dot sheets are determined using the short-range model of quantum dot. The density of states and spectral dependencies of the anisotropic absorption coefficient under midinfrared transitions from doped quantum dots into miniband states of a superlattice strongly depend on dot concentration and on the period of sheets. These dependencies can be used for the characterization of the multilayer structure and they determine the parameters of different optoelectronic devices exploiting the vertical transport of carriers through quantum-dot sheets.

DOI: 10.1103/PhysRevB.85.235321 PACS number(s): 73.21.Cd, 73.21.La, 78.67.Pt

I. INTRODUCTION

Heterostructures formed by quantum-dot (QD) sheets are widely investigated and used in different devices, such as lasers, photodetectors, and solar cells, see Refs. 1,2, and 3 for review. In such heterostructures, not only should the additional localized states of electrons captured into QDs be taken into account, but also the continuous electronic states, which are subjected to reflections on periodically placed QD sheets, which should be modified significantly. Such a periodical perturbation gives rise to a superlattice (SL) with an energy spectrum formed by gaps between the allowed minibands. In contrast to the standard case,[4] an additional damping of electronic states takes place due to scattering on inhomogeneities of QD sheets stemming from a random in-plane distribution of QDs. But such a damping appears to be weak for the low-energy region. As a result, the SL effect should be essential near the edge of the interband absorption in the host material, which is proportional to the density of states of the SL, or under IR transitions from doped QDs into miniband states. To the best of our knowledge, these phenomena were not considered based on a simultaneous description of SL minibands and damping effects in spite of the fact that the structures under consideration are routinely used in different optoelectronic devices. At the same time the opposite case of three-dimensional (3D) ordering of the closely spaced QDs, when a SL is formed as a result of the tunneling mix between intra-QD states, was analyzed[5] and demonstrated experimentally, see Refs. 6 and 7 and references therein. Because of this, it is important and timely to develop an adequate theory of low-energy electrons interacting with the periodically placed QD sheets and to study the optical response of a SL which can be used for the characterization of structures under consideration and for a description of different optoelectronic devices.

In this paper we study low-energy electronic states, with energies in the vicinity of the conduction band extremum, in heterosrtuctures formed by QD sheets of period l using the effective-mass equations for the Green's function averaged over randomly placed QDs in each sheet. In contrast to the standard theoretical description based on the averaging over 3D or two-dimensional (2D) space,[8] here we perform the averaging over QD sheets with the identical statistical characteristics. As a result, we obtain the inhomogeneous along the SL axis Dyson equation where the self-energy function can be replaced by the boundary conditions at QD sheets. Since the damping of the low-energy states is weak, one can consider a SL the characteristics of which are determined by an effective potential localized at the sheet positions $z = nl$, $n = 0, \pm 1, \ldots$. The strength of this potential is determined by the concentration of QDs and the shape of the QD potential. With respect to low-energy states, QD can be considered as a short-range defect (which has been widely investigated over the past 50 years, see Ref. 9) if the low-energy interval under consideration is smaller than the QD binding energy.

The density of states in a SL depends on the period l and on the parameter determined by a strength of the QD's potential described within the short-range approximation. Spectral dependencies of interband absorption between the heavy-hole and SL states are proportional to the density of states in the c band. In addition, the anisotropic absorption coefficient, originated due to mid-IR transitions from the doped QD ground state into the miniband states of SL, is obtained through the QD concentration and the SL parameters. We found that the efficiency of mid-IR photoexcitation is comparable to the contribution of wetting layers formed under QD sheets[10] if the doping levels are the same. But the spectral dependencies are very different for these two mechanisms. Thus, it is demonstrated that the results obtained can be used for the characterization of the structure under consideration. It is more important that the SL parameters determine a mechanism of vertical transport for underbarrier electrons, which is a key process in different optoelectronic devices exploiting multi-QD sheets. A similar mechanism of transport through underbarrier states of IR photodetectors formed by GaAs/AlGaAs-based SL was considered in Ref. 11.

The paper is organized as follows. In Sec. II we describe the model of periodical sheets formed by randomly placed QDs and evaluate the Green's function averaged over random positions of QDs. SL effects on the density of states and on the process of anisotropic photoexcitation of QDs are considered in Sec. III. A list of assumptions used and concluding remarks are presented in the last section. The Appendix contains the

justification of the effective SL approach employed in the calculations performed.

II. MODEL

The electronic states near the c-band extremum of a heterostructure, which is formed by QD sheets placed in the host material, are described by the effective mass Hamiltonian

$$\hat{H} = \frac{\hat{p}^2}{2m} + \sum_{rk} u(\mathbf{r} - \mathbf{R}_{rk}), \tag{1}$$

where $\hat{\mathbf{p}}$ is the 3D momentum operator, m is the effective mass, and $u(\mathbf{r} - \mathbf{R}_{rk})$ is the potential energy of a QD placed at coordinates $\mathbf{R}_{rk} = (\mathbf{x}_{rk}, rl)$. Here r labels the sheet ($r = 0, \pm 1, \pm 2, \ldots$) placed with the period l and k stands for the position of QD over the rth sheet given by a 2D random coordinate $\mathbf{x}_{rk}$ ($k = 1, 2, \ldots, N$ where N is the number of QDs over each sheet with the normalization area L^2). The electron of energy E is described by the Green's function $\mathcal{G}_E(\mathbf{r}, \mathbf{r}')$ governed by the equation

$$(E + i\lambda - \hat{H})\mathcal{G}_E(\mathbf{r}, \mathbf{r}') = \delta(\mathbf{r} - \mathbf{r}') \tag{2}$$

with $\lambda \to +0$ and the 3D δ function $\delta(\Delta\mathbf{r})$. Below we consider the averaged over all QD positions Green's function $G_E(\mathbf{r}, \mathbf{r}') = \langle \mathcal{G}_E(\mathbf{r}, \mathbf{r}') \rangle$ where the averaging over the rth sheet is performed according to[8]

$$\langle \ldots \rangle_r = \frac{1}{L^{2N}} \int d\mathbf{x}_{r1} \cdots \int d\mathbf{x}_{rN} \cdots \tag{3}$$

and $\langle \ldots \rangle$ includes the averaging over all sheets.

Using the $(\mathbf{p}, z)$ representation ($\mathbf{p}$ is 2D momentum) one obtains the Dyson equation governing the averaged Green's function as follows

$$G_{Ep}(z, z') = g_{Ep}(z - z') + \int dz_1 \int dz_2 g_{Ep}(z - z_1) \times \Sigma_{Ep}(z_1, z_2) G_{Ep}(z_2, z'). \tag{4}$$

Here $g_{Ep}(z - z')$ is the free Green's function which is governed by Eq. (2) with the Hamiltonian $\hat{p}^2/2m$, so that

$$g_{Ep}(\Delta z) = \frac{1}{\hbar} \sqrt{\frac{m}{2(\varepsilon_p - E)}} \exp\left(-\frac{\sqrt{2m(\varepsilon_p - E)}\Delta z}{\hbar} \right), \tag{5}$$

if $\varepsilon_p > E$ and the imaginary factor $i\sqrt{E - \varepsilon_p}$ should be used in Eq. (5) if $\varepsilon_p < E$. Within the self-consistent Born approximation, the self-energy function $\Sigma_{Ep}(z_1, z_2)$ in Eq. (4) is given by

$$\Sigma_{Ep}(z_1, z_2) \simeq \frac{n_{\mathrm{QD}}}{L^2} \sum_{r\mathbf{p}_1} u\left(\frac{\mathbf{p} - \mathbf{p}_1}{\hbar}, z_1 - rl \right) \times G_{Ep_1}(z_1, z_2) u\left(\frac{\mathbf{p}_1 - \mathbf{p}}{\hbar}, z_2 - rl \right) + \cdots, \tag{6}$$

where $u(\mathbf{q}, z)$ is the 2D Fourier transform of $u(\mathbf{r})$ and n_{QD} is the QD concentration over a sheet which is not dependent on r (i.e., we consider identical QD sheets).

Further, we restrict ourselves by the low-energy region where scattering on a QD can be described by the short-range potential $u(\mathbf{r}) \approx U\Delta(\mathbf{r})$ with the form factor $\Delta(\mathbf{r})$ localized in volume $\sim a^3$ (a stands for the characteristic size of QD). We also neglect high-order corrections to the self-energy function (6), see the diagram expansion of Fig. 4 and the discussion in the Appendix below. Since the kernel (6) is located near QD sheets with $z_{1,2} \sim rl$ and the Green's functions vary over scales $\hbar/\sqrt{2m|E - \varepsilon_p|}$, the integral equation (4) is transformed into the finite-difference one

$$G_{Ep}(z, z') = g_{Ep}(z - z') + \Lambda_{Ep} \sum_r g_{Ep}(z - rl) G_{Ep}(rl, z'). \tag{7}$$

The self-energy function (6) is written here through the factor

$$\Lambda_{Ep} = \frac{n_{\mathrm{QD}}}{L^2} \sum_{\mathbf{p}_1} G_{Ep_1}(rl, rl) \left| \int d\Delta z u\left(\frac{\mathbf{p} - \mathbf{p}_1}{\hbar}, \Delta z \right) \right|^2, \tag{8}$$

which is the same for any QD sheet [we moved $\Sigma_r, \ldots,$ from Eq. (6) to Eq. (7)]. Instead of Eq. (7), one can determine $G_{Ep}(z, z')$ from Eq. (2) with the free Hamiltonian $\hat{p}^2/2m$ and describe the QD sheet effect adding the boundary conditions

$$\frac{\hbar^2}{2m}\left[\frac{d}{dz} G_{Ep}(z, z') \right]_{z=rl-0}^{z=rl+0} = \Lambda_{Ep} G_{Ep}(rl, z'), \qquad G_{Ep}(z, z')\Big|_{z=rl-0}^{z=rl+0} = 0 \tag{9}$$

at sheet positions $z = rl$. This result was evaluated after acting of the operator $E + i\lambda - \hat{p}^2/2m$ on the integral Dyson equation (4) and the subsequent integration of the intergodifferential equation obtained over the QD positions $(rl - 0, rl + 0)$.

Within the second-order Born approximation we use $G_{Ep}(rl, rl) \simeq g_{Ep}(0)$ in the self-consistent equation (8), see Ref. 8 for details, and the momentum-independent factor Λ_E in Eq. (9) takes the form

$$\Lambda_E = \Lambda\left(1 + i\sqrt{\frac{E}{\varepsilon_a}} \right), \quad \Lambda \equiv \frac{n_{\mathrm{QD}}}{2} U^2 \overline{\rho}_{\varepsilon_a}. \tag{10}$$

Here we estimate Λ for the case of short-range defect within the Koster-Slater approach[12] and $\overline{\rho}_E$ is the 3D density of states which is taken at the cutoff energy $\varepsilon_a \sim (\pi\hbar/a)^2/2m$. Since $E \ll \varepsilon_a$, damping of the low-energy states is weak and one can replace the complex boundary condition (9) by the effective potential energy $-\Lambda \sum_r \delta_a(z - rl)$ with $\delta_a(\Delta z)$ localized in the interval $|\Delta z| < a$, so that in the framework of the effective SL approach $G_{Ep}(z, z')$ is governed by the one-dimensional equation

$$(E + i\lambda - \varepsilon_p - \hat{H}_\perp) G_{Ep}(z, z') = \delta(z - z'), \qquad \hat{H}_\perp = \frac{\hat{p}_z^2}{2m} - \Lambda \sum_r \delta_a(z - rl) \tag{11}$$

with the electron effective mass in the GaAs matrix m. Thus, the Green's function is expressed using the standard relation[8] between $G_{Ep}(z, z')$ and the solutions of the eigenstate problem for SL,[13] $\hat{H}_\perp \psi_z^{(np_\perp)} = \varepsilon_{np_\perp} \psi_z^{(np_\perp)}$. The last equation determines the dispersion relations $\varepsilon_{np_\perp}$ and the eigenfunctions

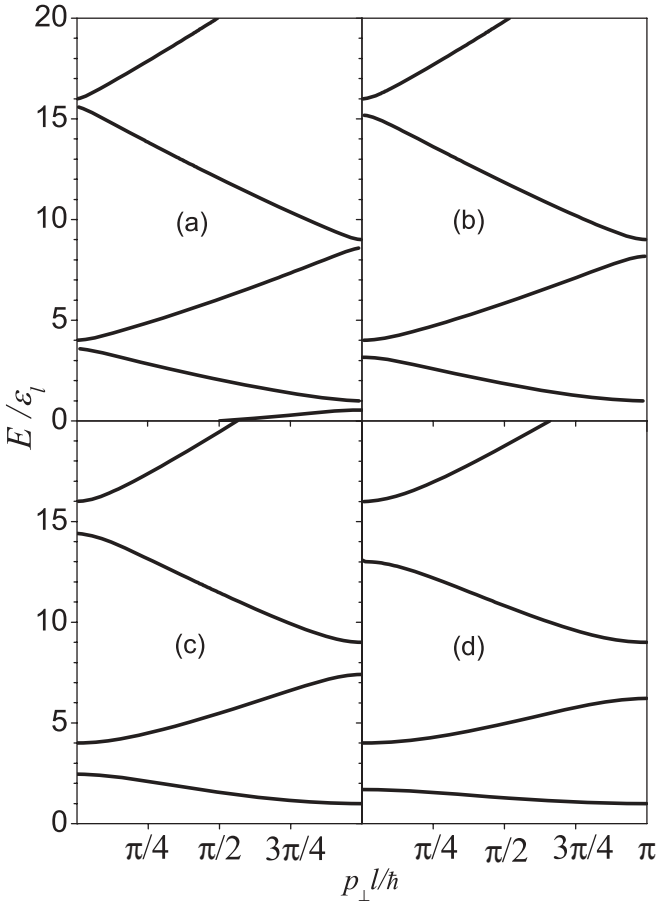

FIG. 1. Miniband energy spectra E/ε_l versus $p_\perp l/\hbar$ of the effective SL determined by Eq. (13) for $Kl = 1$ (a), 2 (b), 4 (c), and 8 (d).

$\psi_z^{(np_\perp)}$. Here $p_\perp$ is quasimomentum ($|p_\perp| < \pi\hbar/l$), n labels minibands, and the wave function takes the form

$$\psi_z^{(np_\perp)} = \psi_{np_\perp}(e^{ik_{np_\perp}z} - R_{np_\perp}e^{-ik_{np_\perp}z}), \tag{12}$$

where the reflection coefficient and the normalization factor $R_{np_\perp}$ and $\psi_{np_\perp}$ are expressed through $p_\perp$ and $k_{np_\perp}$ (Ref. 14). The energy $\varepsilon_{np_\perp} = (\hbar k_{np_\perp})^2/2m$ is founded from the dispersion equation

$$\cos\frac{p_\perp l}{\hbar} = \cos k_{np_\perp} l - \frac{K}{k_{np_\perp}}\sin k_{np_\perp} l, \tag{13}$$

which is written through the characteristic wave vector $K = \Lambda m/\hbar^2 \sim \pi^3 n_{\rm QD} a/2$, see Ref. 13 for details.

The dispersion relations for the lower minibands determined by Eq. (13) are shown in Fig. 1 for dimensionless parameter Kl varied between 1 and 8 when the transformation from the weakly coupled SL (if $Kl \leqslant 2$) to the tight-binding regime of coupling (if $Kl > 4$) takes place. The characteristic energy $\varepsilon_l = (\pi\hbar/l)^2/2m$ is about 3.2 meV for a SL of period $l = 40$ nm. For the SL formed by InAs QDs embedded by a GaAs matrix $Kl \approx 3.1$ if $n_{\rm QD} \simeq 5 \times 10^{10}$ cm^{-2}. As a result, minigaps exceed 5 meV for the tight-binding regime, see Figs. 1(c) and 1(d) when dispersion laws are close to cosine and sine dependencies, for odd and even n, respectively. For the weakly coupled SLs the dispersion laws are formed by parabolic

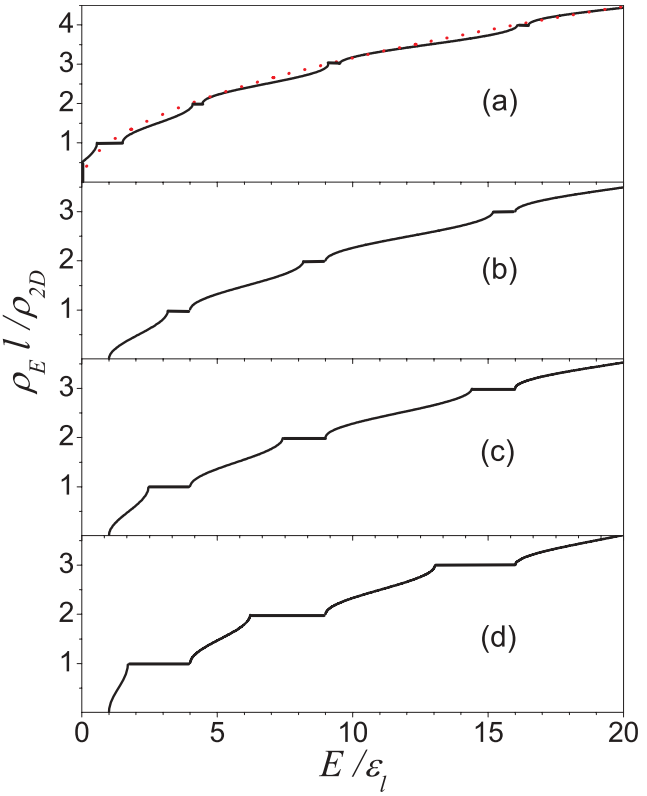

FIG. 2. (Color online) Normalized density of states $\rho_E l/\rho_{2D}$ versus E/ε_l given by Eq. (15) for the parameters used in panels (a–d) of Fig. 1. Dotted curve in upper panel corresponds to the 3D density of states $\propto\sqrt{E}$ if SL effect is negligible, $\Lambda \to 0$.

curves modified near $p_\perp l/\hbar = 0,\pi$ with gaps $\sim$1 meV, see Figs. 1(a) and 1(b). In contrast to a SL corresponding to the underbarrier tunneling regime,[13] if $Kl \leqslant 1.5$ one obtains the lowest miniband at finite $p_\perp l/\hbar$ only, as it is shown in Fig. 1(a). This is because of the absence of a solution for Eq. (13) at $p_\perp \to 0$ and $k_{np_\perp} l \ll 1$. Such a peculiarity changes the density of states and the edge of mid-IR absorption if $Kl \leqslant 1.5$, see Figs. 2(a) and 3(a) below.

III. RESULTS

Using the model described above, we consider in this section the density of states in a SL formed by QD sheets, and calculate the absorption coefficient under mid-IR photoexcitation from ground levels of doped QDs into miniband states of SL.

A. Density of states

The density of states is introduced through the averaged Green's function by the standard formula[8]

$$\rho_E = -\frac{2}{\pi L^3}\mathrm{Im}\int d\mathbf{r}\,\langle \mathcal{G}_E(\mathbf{r},\mathbf{r})\rangle$$
$$\simeq \frac{2}{L^3}\sum_{np_\perp \mathbf{p}}\delta(E - \varepsilon_p - \varepsilon_{np_\perp}), \tag{14}$$

where 2 is due to spin degeneracy and L^3 is the normalization volume. The lower expression is obtained for the case of

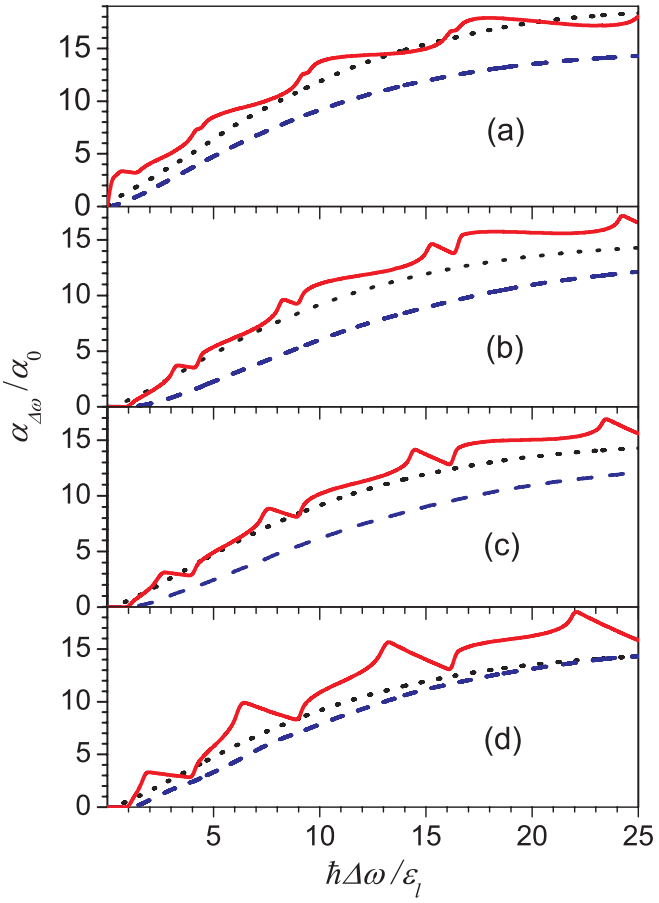

FIG. 3. (Color online) Spectral dependencies of dimensionless absorption coefficients determined by Eqs. (20) and (21) for the same conditions as in Figs. 1 and 2. Solid and dashed curves correspond to the perpendicular and parallel polarizations, respectively. Dotted curves correspond to the case $\Lambda \to 0$, when the SL effect is negligible.

negligible damping in Eq. (10) using the effective SL approach determined by Eqs. (11) to (13), see the energy spectra plotted in Fig. 1. The integration of the δ function over $\mathbf{p}$ gives the 2D density of states ρ_{2D}, and after the integration of the θ function over $p_\perp$ the density of states should be replaced by a constant if E belongs to the $\bar{n}$th gap. In the $\bar{n}$th miniband (below the $\bar{n}$th gap), the integral over $p_\perp$ should be taken over the interval $(0, p_E)$ where p_E is found as a root of the equation $E = \varepsilon_{\bar{n}p_E}$. As a result, ρ_E takes the form

$$\rho_E = \frac{\rho_{2D}}{l}\begin{cases}\bar{n}, & E \subset \bar{n}\text{th gap},\\ \bar{n}-1+p_E l/(\pi\hbar), & E \subset \bar{n}\text{th band},\end{cases} \quad (15)$$

and a shape of ρ_E is determined by the gap-induced steps with the transitions between them determined by the miniband dispersion laws.

In Fig. 2 we plot the dimensionless density of states, in units ρ_{2D}/l, for the same parameters as in Fig. 1. For the weak coupling regime, the jump of ρ_E at $E \to 0$ appears due to the cutoff of the lowest miniband at finite $p_\perp l/\hbar$ [cf. Figs. 1(a) and 2(a) at $E/\varepsilon_l \leqslant 2$]. With the increasing of Kl under transition to the tight-binding regime, the energy-independent gap contributions to the density of states' increase and ρ_E between these steps is transformed from the $\propto \sqrt{E}$ dependency shown by the dotted curve in Fig. 2(a) to the arccosine dependencies. In addition, the bottom of the lowest subband is shifted to energies $\sim\varepsilon_l$. Since ρ_E is connected directly to the shape of interband optical spectra, see Ref. 13, the step-like dependencies permit one to extract the Kl value which determines the band structure of SL according to Eq. (13).

Let us compare the energy scale of the SL effect, determined by ε_l, and the SL effect due to the wetting layer contribution analyzed in Ref. 10. For the parameters given at the end of Sec. II, one obtains that the contribution of a QD sheet with $n_{\rm QD} = 5\times10^{10}$ cm^{-2} is reduced approximately two times in comparison to the wetting layer effect if levels of electron doping are the same. Thus, an interplay of both mechanisms should take place for $n_{\rm QD} \geqslant 10^{11}$ cm^{-2}. For such a case, the interband optical spectra should be dependent on both the QDs' contributions and the wetting layer contributions.

B. Photoionization

The anisotropic absorption coefficients $\alpha_\omega^{||}$ and $\alpha_\omega^{\perp}$ are determined from the general Kubo formula as follows:

$$\alpha_\omega^{||,\perp} = \frac{8(\pi e)^2}{\sqrt{\epsilon}c\omega L^3}\sum_{\delta\delta'}[f(\varepsilon_\delta) - f(\varepsilon_\delta+\hbar\omega)] \times|(\delta|\mathbf{e}_{||,\perp}\cdot\hat{\mathbf{v}}|\delta')|^2\delta(\varepsilon_\delta-\varepsilon_{\delta'}+\hbar\omega), \quad (16)$$

where ϵ is the dielectric permittivity of the host semiconductor and the matrix element $|(\delta|\mathbf{e}_{||,\perp}\cdot\hat{\mathbf{v}}|\delta')|^2$ corresponds to transitions between the δ and δ' states of energies ε_δ and $\varepsilon_{\delta'}$ under radiation with polarization orts $\mathbf{e}_{||,\perp}$. We use the equilibrium distributions $f(\varepsilon_\delta)\to 1$ and $f(\varepsilon_\delta+\hbar\omega)\to 0$ because the only localized states are populated at temperatures lower than the binding energy $|E_0|$. Due to the in-plane isotropy of the problem, we separate the cases of s- and p-polarized radiation corresponding to the polarization orts $\mathbf{e}_\parallel$ and $\mathbf{e}_z$. Neglecting the overlap between QD states and taking the ground state wave functions Ψ_P in the momentum representation ($\mathbf{P}$ is 3D momentum) we transform Eq. (16) into

$$\left|\begin{matrix}\alpha_\omega^{\parallel}\\ \alpha_\omega^{\perp}\end{matrix}\right| = -\frac{4\pi e^2}{\sqrt{\epsilon}c\omega m^2 L^9}\sum_{\mathbf{PP}'}\Psi_P\Psi^*_{P'}\int d\mathbf{r}\int d\mathbf{r}' \times e^{i(\mathbf{Pr}-\mathbf{P}'\mathbf{r}')/\hbar}\left|\begin{matrix}(\mathbf{e}_\parallel\mathbf{P})(\mathbf{e}_\parallel\mathbf{P}')\\ \hat{p}_z\hat{p}^+_{z'}\end{matrix}\right| K_{\Delta\mathbf{p},E_0+\hbar\omega}(\mathbf{r}',\mathbf{r}). \quad (17)$$

The contribution of the miniband states is described here through the average of the exact Green's function $\mathcal{G}_E(\mathbf{r}',\mathbf{r})$ with the exponential factor corresponding to random QD positions (here $\Delta\mathbf{p}\equiv\mathbf{P}-\mathbf{P}'$)

$$K_{\Delta\mathbf{p},E}(\mathbf{r}',\mathbf{r}) = \left\langle\sum_{rk} e^{i\Delta\mathbf{p}\mathbf{R}_{rk}/\hbar}\mathrm{Im}\mathcal{G}_E(\mathbf{r}',\mathbf{r})\right\rangle, \quad (18)$$

which is analyzed in the Appendix. Within the low-order approach, the correlation function (18) takes the form

$$K_{\Delta\mathbf{p},E}(\mathbf{r}',\mathbf{r}) \approx N_{\rm QD}\frac{L}{l}\delta_{\Delta\mathbf{p},0}\mathrm{Im}G_E(\mathbf{r}',\mathbf{r}), \quad (19)$$

where $N_{\rm QD}L/l$ is the total number of QDs in the normalization volume L^3 and the averaged Green's function $G_E(\mathbf{r}',\mathbf{r})$ was considered in Sec. II.

Using the ground state wave function Ψ_P written in the Koster-Slater approach[12] and neglecting the damping correction in Eq. (10) we transform Eq. (17) as follows

$$\left|\begin{matrix}\alpha_\omega^{\parallel}\\ \alpha_\omega^{\perp}\end{matrix}\right| = \frac{(2\pi e)^2 n_{\rm QD}}{\sqrt{\epsilon}c\omega m^2 l L^3}\sum_{\mathbf{p}p_\perp}|\Psi_P|^2\left|\begin{matrix}p^2/2\\ p_\perp^2\end{matrix}\right| \times\sum_{n\bar{p}_\perp}\left|\frac{2}{l}\int_{-l}^{l}dz e^{-ip_\perp z/\hbar}\psi_z^{(n\bar{p}_\perp)}\right|^2\delta(\hbar\Delta\omega-\varepsilon_{n\bar{p}_\perp}-\varepsilon_p). \tag{20}$$

Here $\mathbf{P}\equiv(\mathbf{p},p_\perp)$ and we have replaced $G_{Ep}(z',z)$ from Eq. (19) using the wave function (12). In the expressions for $\alpha_\omega^{\parallel,\perp}$ integrals over the $\mathbf{p}$ plane and over z are taken analytically and the spectral dependencies of IR absorption are obtained after the double numerical integrations over the transverse momenta $p_\perp$ and $\bar{p}_\perp$. The dimensionless spectral dependencies are plotted in Fig. 3 for the same conditions as in Figs. 1 and 2. The characteristic absorption α_0 is given by

$$\alpha_0 = \frac{(4e)^2 n_{\rm QD}}{c\sqrt{\epsilon m|E_0|/2}}\left(\frac{\varepsilon_l}{E_0}\right)^2 \tag{21}$$

and $\alpha_0\sim 3\ {\rm cm}^{-1}$ for the above listed parameters. Thus, for the maximal absorption, when $\hbar\Delta\omega/\varepsilon_l\sim 20$–$30$ or $\hbar\Delta\omega\sim|E_0|$, one obtains $\alpha_{\max}\sim 45\ {\rm cm}^{-1}$. Since $\alpha_\omega^{\parallel,\perp}\propto n_{\rm QD}/l^4$, the maximal absorption increases up to $\alpha_{\max}\geqslant 10^3\ {\rm cm}^{-1}$ if $n_{\rm QD}>10^{11}\ {\rm cm}^{-2}$ and $l\simeq 20$ nm; an approximation of low QD concentration remains valid for such a set of parameters. The further increase of $\alpha_{\max}$ is possible in the case of heavily doped SL, with a few electrons captured in QD.

Anisotropy of absorption is about 20% without any strong dependency on the effective potential [cf. Figs. 3(a) to 3(d) where parameter Kl varies from 1 to 8]. The peculiarities of miniband spectra are visible clearly in $\alpha_\omega^{\perp}$ starting from $Kl\geqslant 2$ while $\alpha_\omega^{\parallel}$ does not show any peculiarities at the edges of minibands. This is due to different selection rules for transverse and longitudinally polarized excitations: in the last case, transitions are forbidden at the edges of minibands and the spectral dependencies remain smooth. In addition, Fig. 1(a) shows a jump of $\alpha_\omega^{\perp}$ at $\hbar\Delta\omega=0$ which is similar to the jump of the density of states in Fig. 2(a) (we do not consider IR transitions into shallow underbarrier states at $\hbar\Delta\omega<0$). In Figs. 3(b) to 3(d), shifts of absorption edges to finite $\hbar\Delta\omega>0$ take place due to lower miniband shifts, see Figs. 1(b) to 1(d) and 2(b) to 2(d).

IV. CONCLUSION

In summary, we have developed the theory of the superlattice formed by periodically placed quantum-dot sheets. It was found that the damping due to random in-plane positions of dots is weak and the effect of the sheets on electronic states can be described using the effective boundary conditions. Within this approach we have demonstrated that the miniband density of states, which describes the interband absorption, and spectra of mid-IR photoexcitation of doped quantum dots into minibands strongly depend on the parameters of the quantum-dot sheets. Visible anisotropy of the absorption coefficient is also found, with transverse absorption which is strongly modulated by the miniband spectrum of SL.

Now we discuss the main assumptions in the calculations performed. We restricted ourselves by the vicinity of the c band using the effective-mass approach in Eq. (1) and in further consideration of the photoionization process. To describe the energy intervals comparable to the gap, one needs to use the multiband $\mathbf{kp}$ Hamiltonian for a more detailed description of QD states.[15] We consider the case of low QD concentration ($n_{\rm QD}/l\sim 10^{15}\ {\rm cm}^{-3}$ in our numerical estimates) and the electron-electron interaction effect on the energy spectrum; thus, the IR absorption should be weak. Numerical estimates for the SL parameters were performed here based on a simplified description of QD as an isotropic short-range defect with the binding energy corresponding to typical QD. This approach gives approximate SL parameters only and a more precise description should be based on a numerical solution of the self-consistent Dyson equation taking into account a real potential of QD.[1,15] Because parameters of a QD sheet (materials, concentration, and shape of QD) can be very different, such a consideration should be performed for different specific cases (e.g., for Ge/Si-based or $A_{II}B_{VI}$-based QD sheets, for review see Ref. 16).

To conclude, we believe that the results obtained will stimulate an investigation of underbarrier vertical transport of carriers to verify the SL effect on electronic properties of structures formed by QD sheets. The spectral and polarization dependencies of the mid-IR photoexcitation are convenient for direct measurements because the valence band states are not essential. These results should be important for a description of different devices utilizing periodical QD sheet structures.

ACKNOWLEDGMENT

This work was supported by the AFOSR.

APPENDIX

To estimate the corrections beyond the effective potential approach used in Eqs. (9) to (11) we consider here the method of calculations in more detail. Using the $\mathbf{p}z$ representation, one obtains the self-consistent Dyson equation (4) for the averaged Green's function $G_{Ep}(z,z')$ shown by a bold line as it is plotted in Fig. 4. Within the second-order Born approximation, we use the free Green's function in the self-energy function (6) given by the first diagram of the set for Σ_{Ep} shown in the lower line of Fig. 4. The next correction in this set can be neglected under the standard condition[8]

$$E\gg|\Sigma_{Ep}|\simeq\Lambda \tag{A1}$$

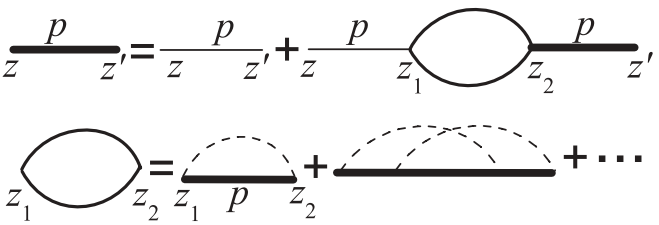

FIG. 4. Self-consistent Dyson equation for averaged Green's function $G_{Ep}(z,z')$ and the self-energy function $\Sigma_{Ep}(z_1,z_2)$ shown in upper and lower lines, respectively.

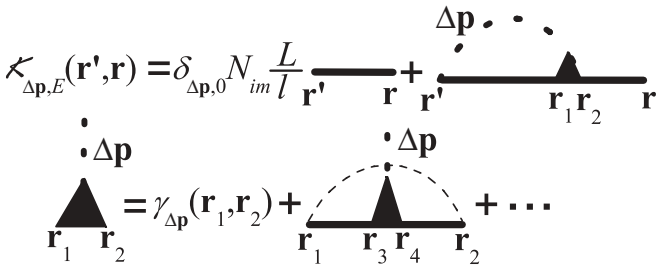

FIG. 5. Diagram expansion for correlation function $\mathcal{K}_{\Delta\mathbf{p}E}(\mathbf{r},\mathbf{r}')$ written through the diagram set for the vertex part shown in lower line.

and we arrive at Eq. (7) using the free Green's function in Σ_{Ep} determined by Eq. (6).

More complicated consideration is necessary for the correlation function $K_{\Delta\mathbf{p}E}(\mathbf{r},\mathbf{r}')$ appearing in Eq. (17) because of the random factor $\exp(i\,\Delta\mathbf{p}\mathbf{R}_{rk}/\hbar)$ describing positions of QDs. Instead of Eq. (18) it is convenient to consider the generalized expression

$$\mathcal{K}_{\Delta\mathbf{p},E}(\mathbf{r}',\mathbf{r}) = \left\langle \sum_{rk} e^{i\,\Delta\mathbf{p}\mathbf{R}_{rk}/\hbar}\mathcal{G}_E(\mathbf{r}',\mathbf{r}) \right\rangle, \qquad \text{(A2)}$$

which is shown in Fig. 5. Here a dotted curve corresponds to the averaged factor

$$\left\langle \sum_{r_1k_1r_2k_2} \exp\left(-\frac{i}{\hbar}\Delta\mathbf{p}\cdot\mathbf{R}_{r_1k_1}\right) u(\mathbf{r}-\mathbf{R}_{r_2k_2}) \right\rangle, \qquad \text{(A3)}$$

while the dashed curves in Figs. 4 and 5 stand for the paired QD potentials. After summation over all reducible diagrams, $K_{\Delta\mathbf{p}E}(\mathbf{r},\mathbf{r}')$ is written through the averaged Green's function and the vertex part, which is given by the set shown in the lower line of Fig. 5 with the initial vortex determined from Eq. (A3) as follows

$$\gamma_{\Delta\mathbf{p}}(\mathbf{r}_1,\mathbf{r}_2) = n_{\mathrm{QD}} \sum_r u\left(-\frac{\Delta\mathbf{p}}{\hbar}, z_1 - rl\right) \times e^{-\frac{i}{\hbar}(\Delta\mathbf{p}\mathbf{x}_1 + rp_\perp l)}\delta(\mathbf{r}_1-\mathbf{r}_2). \qquad \text{(A4)}$$

The first correction to Eq. (19) appears, if we use (A4), as the vertex part in the diagram expansion for the correlation function shown in Fig. 5. Performing straightforward calculations under the condition (A1), one obtains that this correction and the next contributions are negligible in comparison with Eq. (19).

*fedirvas@buffalo.edu

[1] D. Bimberg, M. Grundmann, and N. N. Ledentsov, *Quantum Dot Heterostructures* (J. Wiley and Sons, New York, 1999); A. A. Lagatsky, C. G. Leburn, C. T. A. Brown, W. Sibbett, S. A. Zolotovskaya, and E. U. Rafailov, Prog. Quantum Electron. **34**, 1 (2010).

[2] A. V. Barve, S. J. Lee, S. K. Noh, and S. Krishna, Laser Photonics Reviews **4**, 738 (2010); A. Rogalski, J. Antoszewski, and L. Faraone, J. Appl. Phys. **105**, 091101 (2009); S. D. Gunapala, S. V. Bandara, S. B. Rafol, and D. Z. Ting, Semicond. Semimet. **84**, 59 (2011).

[3] A. J. Nozik, M. C. Beard, J. M. Luther, M. Law, R. J. Ellingson, and J. C. Johnson, Chem. Rev. **110**, 6873 (2010); E. U. Rafailov, M. A. Cataluna, and W. Sibbett, Nature Photonics **1**, 395 (2007).

[4] M. Steslicka, R. Kucharczyk, A. Akjouj, B. Djafari-Rouhani, L. Dobrzynski, and S. G. Davison, Surf. Sci. Rep. **47**, 93 (2002).

[5] D. L. Nika, E. P. Pokatilov, Q. Shao, and A. A. Balandin, Phys. Rev. B **76**, 125417 (2007); O. L. Lazarenkova and A. A. Balandin, *ibid.* **66**, 245319 (2002).

[6] M. Buljan, U. V. Desnica, M. Ivanda, N. Radic, P. Dubcek, G. Drazic, K. Salamon, S. Bernstorff, and V. Holy, Phys. Rev. B **79**, 035310 (2009); D. Grutzmacher, T. Fromherz, C. Dais, J. Stangl, E. Muller, Y. Ekinci, H. H. Solak, H. Sigg, R. T. Lechner, E. Wintersberger, S. Birner, V. Holy, and G. Bauer, Nano Lett. **7**, 3150 (2007); M. V. Artemyev, A. I. Bibik, L. I. Gurinovich, S. V. Gaponenko, and U. Woggon, Phys. Rev. B **60**, 1504 (1999).

[7] S. Kiravittaya, A. Rastelli, and O. G. Schmidt, Rep. Prog. Phys. **72**, 046502 (2009).

[8] G. D. Mahan, *Many-Particle Physics* (Plenum, New York, 1990); F. T. Vasko and O. E. Raichev, *Quantum Kinetic Theory and Applications* (Springer, New York, 2005).

[9] G. Lukovsky, Solid State Commun. **3**, 299 (1965); A. M. Stoneham, *Theory of Defects in Solids* (Oxford University Press, Oxford, 2001).

[10] R. Pickenhain, H. Schmidt, and V. Gottschalch, J. Appl. Phys. **88**, 948 (2000); F. T. Vasko and V. V. Mitin, arXiv:1110.0744 (unpublished).

[11] S. D. Gunapala, B. F. Levine, and N. Chand, J. Appl. Phys. **70**, 305 (1991); M. Helm, Semicond. Sci. Technol. **10**, 557 (1995).

[12] Using the Koster-Slater approach (Ref. 9) one can find the binding energy of the short-range defect E_0 from the equation

$$1 + U\overline{\rho}_{\varepsilon_a} = \pi U\overline{\rho}_{E_0}/2$$

and the normalized wave function of the ground state Ψ_P used in Eqs. (17) and (20) is given by

$$\Psi_P = \frac{2\sqrt{E_0/2\rho_{E_0}}}{E_0+\varepsilon_P}.$$

[13] M. Herman, *Semiconductor Superlattices* (Academie-Verlag, Berlin, 1986); F. T. Vasko and A. Kuznetsov, *Electronic States and Optical Transitions in Semiconductor Heterostructures* (Springer, New York, 1998).

[14] According to the authors of Ref. 13, the explicit expressions for the reflection coefficient $R_{np_\perp}$ and the normalization factor $\psi^2_{np_\perp}$ are written as

$$R_{np_\perp} = \frac{\exp(ip_\perp l/\hbar) - \exp(ik_{np_\perp}l)}{\exp(ip_\perp l/\hbar) - \exp(-ik_{np_\perp}l)}$$

and

$$2l\psi^2_{np_\perp} = [1-\cos(p_\perp l/\hbar + k_{np_\perp}l)]\left\{1 - \frac{\sin(2k_{np_\perp}l)}{2k_{np_\perp}l} - \cos\frac{p_\perp l}{\hbar}\left[\cos(k_{np_\perp}l) - \frac{\sin(k_{np_\perp}l)}{k_{np_\perp}l}\right]\right\}^{-1}.$$

[15] O. Stier, M. Grundmann, and D. Bimberg, Phys. Rev. B **59**, 5688 (1999); F. Boxberg and J. Tulkki, Rep. Prog. Phys. **70**, 1425 (2007).

[16] A. D. Yoffe, Adv. Phys. **50**, 1 (2001).